








RESEARCH ARTICLE

A structural investigation of organic battery anode materials by NMR crystallography

Tommy Whewell¹ | Valerie R. Seymour^{1,2}  | Kieran Griffiths¹  |
 Nathan R. Halcovitch¹  | Aamod V. Desai^{2,3}  | Russell E. Morris^{2,3}  |
 A. Robert Armstrong^{2,3}  | John M. Griffin^{1,2,4} 

¹Department of Chemistry, Lancaster University, Lancaster, UK

²The Faraday Institution, Quad One, Harwell Science and Innovation Campus, Didcot, UK

³EastChem School of Chemistry, University of St Andrews, St Andrews, UK

⁴Materials Science Institute, Lancaster University, Lancaster, UK

Correspondence

John M. Griffin, Department of Chemistry, Lancaster University, Lancaster, LA1 4YB, UK.
 Email: j.griffin@lancaster.ac.uk

Funding information

Engineering and Physical Sciences Research Council, Grant/Award Numbers: EP/M022501/1, EP/P0201194, EP/P025561/1, EP/R029946/1, EP/T015063/1, EP/P020194; Leverhulme Trust, Grant/Award Numbers: DS-2017-036, RPG-2018-395; Faraday Institution, Grant/Award Number: FIRG018

Abstract

Conjugated alkali metal dicarboxylates have recently received attention for applications as organic anode materials in lithium- and sodium-ion batteries. In order to understand and optimise these materials, it is important to be able to characterise both the long-range and local aspects of the crystal structure, which may change during battery cycling. Furthermore, some materials can display polymorphism or hydration behaviour. NMR crystallography, which combines long-range crystallographic information from diffraction with local information from solid-state NMR via interpretation aided by DFT calculations, is one such approach, but this has not yet been widely applied to conjugated dicarboxylates. In this work, we evaluate the application of NMR crystallography for a set of model lithium and sodium dicarboxylate salts. We investigate the effect of different DFT geometry optimisation strategies and find that the calculated NMR parameters are not systematically affected by the choice of optimisation method, although the inclusion of dispersion correction schemes is important to accurately reproduce the experimental unit cell parameters. We also observe hydration behaviour for two of the sodium salts and provide insight into the structure of an as-yet uncharacterised structure of sodium naphthalenedicarboxylate. This highlights the importance of sample preparation and characterisation for organic sodium-ion battery anode materials in particular.

1 | INTRODUCTION

In recent decades, batteries have held an increasing importance in everyday life. Lithium-ion batteries are now well established in society with a growing focus on green-tech applications, including electric vehicles, and demand is set to increase further. As their usage increases, there are concerns surrounding the ethics and

sustainability of the raw materials used, which is driving development of new battery chemistries. One aspect concerns the development of new chemistries based on more sustainable charge carrying ions such as sodium, which is seen as a low-cost alternative to lithium due to its much higher abundance. Another goal is to increase the sustainability of other aspects of battery chemistry. In this respect, organic compounds based on layered

This is an open access article under the terms of the Creative Commons Attribution License, which permits use, distribution and reproduction in any medium, provided the original work is properly cited.

© 2022 The Authors. *Magnetic Resonance in Chemistry* published by John Wiley & Sons Ltd.

conjugated carboxylate salts have gained interest in recent years as potential anode materials for lithium and sodium batteries. In principle, these organic coordination polymers can be derived from green and sustainable sources or from recycled waste plastic.^[1,2]

Demonstrated by Armand et al.,^[3] one of the first candidate organic anode materials was lithium benzenedicarboxylate (Li₂BDC). This lithium salt can undergo reversible lithiation by rearrangement of the π -electron conjugation system to incorporate two further Li⁺ ions per formula unit, resulting in a formula of Li₄BDC. This reaction occurs at 0.8 V versus Li⁺/Li⁰ and gives a specific capacity of 300 mA h g⁻¹. More recently, sodium dicarboxylates have also shown promising properties for sodium-ion batteries. Zhao et al.^[4] demonstrated that sodium benzenedicarboxylate (Na₂BDC) can also reversibly intercalate Na⁺ ions with a capacity of 250 mA h g⁻¹ at a voltage of 0.4 V versus Na⁺/Na⁰. Park et al.^[5] subsequently demonstrated that Na₂BDC can exhibit rate performance equivalent to commercial LIBs.

As interest in organic anode materials has increased, a number of systematic studies have attempted to gain insight into their reduction mechanisms and structure–property relationships. It has been demonstrated that increasing the length of the conjugation system of the organic backbone can improve cycling stability as a result of increased electronic conductivity.^[6–10] This effect can be seen when comparing benzenedicarboxylate-based molecules with biphenyldicarboxylate-based molecules such as lithium biphenyldicarboxylate (Li₂BPDC).^[11] However, the drawback to increasing the length and molecular weight of the organic backbone is that this reduces the specific capacity of the material. This can be partially mitigated by using directly adjacent ring systems, such as those found in naphthalene.^[10,12–14] Lithium naphthalene dicarboxylate (Li₂NDC) and sodium naphthalene dicarboxylate (Na₂NDC) both feature two rings in the organic component of the structure, while possessing a lower molecular weight than the biphenyldicarboxylate analogues.

Despite the progress that has been made in understanding structure–property relationships in organic anodes, there is still no clear consensus on the precise structural details of the reduction mechanisms. In order to understand these, it is necessary to have a detailed understanding of the crystal structure and to have characterisation methods that are capable of probing both the long-range and local structure. The crystal structures of many organic anode materials are known from single-crystal X-ray diffraction (SCXRD), but some salts can display complicated hydration behaviour or polymorphism. For studying battery cells, it is also important to have

techniques that are capable of providing atomic-level structural information for powder samples that are used in electrode formulations. Powder X-ray diffraction (PXRD) can provide information on the long-range structure but can be less sensitive to small changes in local structure, particularly involving light elements such as lithium. In contrast, solid-state NMR spectroscopy provides limited information on the long-range structure but is highly sensitive to the local chemical environment and can provide information about disorder and dynamics. The information from solid-state NMR can be linked with long-range crystallographic information from diffraction through density functional theory (DFT) calculations under periodic boundary conditions. In recent years, the combination of NMR, XRD and DFT in this way has been termed NMR crystallography, and this approach has seen widespread application to a large range of materials.^[15–17]

In this work, we present a systematic study of model organic anode materials for lithium and sodium batteries using NMR crystallography. The purpose of this work is to evaluate the use of NMR crystallography for a set of materials which share common structural features and interactions, with a view to its future application for the study of structural changes upon lithiation and sodiation. A key consideration in organic conjugated carboxylates is the presence of weak non-bonding interactions between ligands, which are not well accounted for by standard DFT approaches. We therefore consider a range of different DFT structural optimisation methods, including semi-empirical dispersion correction (SEDC), and evaluate the effect on the optimised crystal structure and calculated NMR parameters. We find that the choice of optimisation method can have a measurable effect on the unit cell parameters and atomic positions from the point of view of PXRD but that, in most cases, the effect on the local structure is small and calculated NMR parameters are relatively insensitive to the optimisation method used. Our results also provide insight into the hydration behaviour of two salt forms which have as yet uncharacterised structures.

2 | EXPERIMENTAL DETAILS

2.1 | Synthesis

Lithium benzenedicarboxylate (Li₂BDC) was synthesised following a procedure adapted from that reported by Armand et al.^[3] An aqueous solution (20 ml) of LiOH (0.53 g, 22.20 mmol) was combined with a solution of terephthalic acid (1.03 g, 6.22 mmol) in ethanol (50 ml). The combined solution was stirred at reflux conditions

for 12 h. The resulting milky solution was washed with ethanol yielding a white powder, which was filtered and then dried for 24 h at 120°C in vacuo.

Lithium naphthalenedicarboxylate (Li_2NDC) was synthesised following a procedure adapted from that reported by Yasuda and Ogihara^[13] and Ogihara et al.^[18] Methanol (100 ml) was added to an aqueous solution (0.23 ml) of LiOH (0.33 g, 13.78 mmol). 2,6-naphthalenedicarboxylic acid (0.98 g, 4.53 mmol) was added rapidly under stirring. The solution was stirred at reflux conditions for 12 h. The resulting white solid was filtered, washed with methanol and dried at 120°C in vacuo for 24 h.

Lithium biphenyldicarboxylate (Li_2BPDC) was synthesised following a procedure adapted from that reported by Choi et al.^[11] for the synthesis of sodium biphenyldicarboxylate. An aqueous solution (50 ml) of 4,4-biphenyldicarboxylic acid (4.80 g, 19.82 mmol) was combined with an aqueous solution (15 ml) of LiOH (1.40 g, 58.46 mmol) under stirring. This solution was stirred for 12 h at ambient temperature. The resulting precipitate was filtered, washed with ethanol and dried for 24 h at 120°C in vacuo.

Sodium benzenedicarboxylate (Na_2BDC) was synthesised following a procedure adapted from that reported by Kaduk.^[19] Terephthalic acid (1.73 g, 10.41 mmol) was added to a warm aqueous solution (5 ml) of NaOH (1.38 g, 34.50 mmol). Deionised water (40 ml) was added until the acid dissolved, at which point ethanol (30 ml) was added slowly to the clear solution at 80°C until a precipitate formed. This mixture was then stirred at reflux conditions for 2 h. The resultant suspension was filtered, washed with ethanol and dried at 120°C in vacuo.

Sodium naphthalenedicarboxylate (Na_2NDC) was synthesised following a procedure adapted from that reported by Ogihara et al.^[12] and Cabañero et al.^[14] NaOH (0.25 g, 6.25 mmol) was dissolved in methanol (50 ml); to this solution, 2,6-naphthalenedicarboxylic acid (0.50 g, 2.31 mmol) was added rapidly under stirring. The solution was stirred at reflux conditions for 24 h. The resulting solution was filtered, washed with methanol and dried at 120°C in vacuo.

Sodium naphthalene dicarboxylate tetrahydrate ($\text{Na}_2\text{NDC}\cdot 4\text{H}_2\text{O}$) was synthesised following a procedure adapted from that reported by Ogihara et al.^[12] and Cabañero et al.^[14] 2,6-naphthalene dicarboxylic acid (0.50 g, 2.31 mmol) was added to a warm aqueous solution of NaOH (0.2 g, 5.00 mmol). Methanol was added (5 ml) and the resulting solution stirred for 30 min. The mixture was then exposed to acetone vapour inside a refrigerator, and single-crystals were extracted after 2 weeks.

Sodium biphenyldicarboxylate (Na_2BPDC) was synthesised following a procedure adapted from that reported by Choi et al.^[11] An aqueous solution (50 ml) of 4,4-biphenyldicarboxylic acid (2.40 g, 9.91 mmol) was combined with an aqueous solution (15 ml) of NaOH (1.20 g, 30.00 mmol) and stirred for 12 h at ambient temperature. The resulting precipitate was filtered, washed with ethanol and dried for 24 h at 120°C in vacuo.

Sodium biphenyldicarboxylate monohydrate ($\text{Na}_2\text{BPDC}\cdot\text{H}_2\text{O}$) was synthesised following a procedure adapted from that reported by Choi et al.^[11] An aqueous solution (13 ml) of 4,4-biphenyldicarboxylic acid (1.02 g, 4.21 mmol) was added to an aqueous solution (9 ml) of NaOH (0.6 g, 15.00 mmol). The resulting solution was exposed to ethanol vapours inside a refrigerator. Crystals began to appear within 3 weeks and were extracted after 4 weeks before being dried in air.

2.2 | Diffraction details

Single crystals were mounted on a Mitegen loop using Paratone-N oil and were analysed using an Rigaku Oxford Diffraction SuperNova diffractometer equipped with an Atlas S2 CCD detector using $\text{CuK}\alpha$ radiation ($\lambda = 1.54184 \text{ \AA}$). Crystals were kept at 100 K during data collection. Using Olex2,^[20] crystal structures were solved with the ShelXT^[21] structure solution programme using Intrinsic Phasing and refined with the SHELXL^[22] package using least-squares minimisation, data collection and integration were performed using CrysAlisPro.

Polycrystalline materials were analysed using powder XRD. Samples were analysed with a Rigaku SmartLab diffractometer equipped with a D/teX-ULTRA 250 High-Speed Position-Sensitive Detector system and a $\text{Ge}(220) \times 2$ 2-bounce monochromator using $\text{CuK}\alpha_1$ radiation ($\lambda = 1.54059 \text{ \AA}$) within a 2θ range of $5\text{--}70^\circ$ (step size of 0.01°).

TABLE 1 CCDC codes for crystal structures used in this work

Structure	CCDC deposition number
Li_2BDC	664607 [23]
Li_2NDC	722281 [24]
Li_2BPDC	757041 [25]
Na_2BDC	145817 [19]
Na_2NDC	N/A [14]
$\text{Na}_2\text{NDC}\cdot 4\text{H}_2\text{O}$	1558952 [26]
$\text{Na}_2\text{BPDC}\cdot\text{H}_2\text{O}$	2120033 (this work) and 944127 [11]

Results of single crystal X-ray diffraction experiments were obtained from the literature for all six dicarboxylate salts. Details can be found in Table 1.

2.3 | NMR details

Unless otherwise stated, solid-state NMR experiments were performed on Bruker Avance III HD spectrometers operating at magnetic field strengths of 9.4 and 16.4 T. ^{13}C NMR spectra are referenced relative to tetramethylsilane using the methyl resonance of *L*-alanine at 20.5 ppm as a secondary reference. ^7Li NMR spectra are referenced relative to 1 M $\text{LiCl}_{(\text{aq})}$ using solid LiCl at -1.2 ppm as a secondary reference. ^{23}Na NMR spectra are referenced relative to 1 M $\text{NaCl}_{(\text{aq})}$ using solid NaCl at 7.4 ppm as a secondary reference.

^{13}C NMR spectra were recorded at a magic-angle spinning (MAS) rate of between 15 and 16 kHz using cross polarisation (CP) to transfer magnetisation from ^1H with a contact time of between 1 and 5 ms. The CP pulse power was ramped linearly from 70% to 100%. ^1H heteronuclear decoupling using two-pulse phase modulation (TPPM)^[27] with a pulse length of 4.8 μs and a radio-frequency field strength of 100 kHz was applied during acquisition. Spectra are the sum of between 64 and 960 transients separated by a recycle interval of between 60 and 120 s.

The ^7Li MAS NMR spectra were recorded at a MAS rate of 5 kHz. Static spectra were recorded using a solid-echo (90° - τ - 90° - τ -acquire) pulse sequence with a 16-step phase cycle. Spectra are the sum of between 64 and 16,384 transients separated by a recycle interval of between 3 and 10 s.

The ^{23}Na MAS NMR spectra were recorded at a MAS rate of 12.5 kHz. Spectra are the sum of between 112 and 408 transients separated by a recycle interval of 3 s.

^{23}Na multiple-quantum (MQ) MAS spectra were recorded at a MAS rate of 12.5 kHz using a split- t_1 pulse sequence. A two-component fast amplitude modulation pulse^[28] was used for conversion of three-quantum to single-quantum coherence. Spectra are the sum of between 192 and 720 transients for each of between 96 and 129 t_1 rows separated by a recycle interval of 3 s.

2.4 | DFT details

First-principles calculations of theoretical NMR parameters were carried out using the CASTEP code^[29] including the gauge-including projector augmented wave (GIPAW) algorithm,^[30] which allows the reconstruction of the all-electron wave function in the presence of a

magnetic field. The CASTEP calculations employed the generalised gradient approximation (GGA) Perdew-Burke-Ernzerhof (PBE) exchange-correlation functional,^[31] and core valence interactions were described by ultrasoft pseudopotentials.^[32] The revised PBE (rPBE) exchange-correlation functional was also used to keep consistency with a methodology reported in the literature.^[33] Prior to the calculation of NMR parameters, structural models from diffraction experiments were geometry optimised using a range of different strategies, including full relaxation and the use of the G06 semi-empirical dispersion correction (SEDC) scheme.^[34]

Geometry optimisations and NMR calculations were carried out using a planewave energy cut off of 50 Ry and a k -point spacing of $0.05\ 2\pi\ \text{\AA}^{-1}$. The calculations generate the absolute shielding tensor (σ) in the crystal frame. Diagonalisation of the symmetric part of σ yields the three principal components, σ_{XX} , σ_{YY} and σ_{ZZ} . The isotropic shielding, σ_{iso} , is given by $(1/3)\text{Tr}[\sigma]$. The isotropic chemical shift, δ_{iso} , is given by $\sigma_{\text{ref}} - \sigma_{\text{iso}}$, where σ_{ref} is a reference shielding determined by comparison of experimental chemical shifts over the complete range of structures. The quadrupolar coupling constant, $C_Q = eQV_{ZZ}/h$ and asymmetry parameter, $\eta_Q = (V_{XX} - V_{YY})/V_{ZZ}$ are obtained directly from the principal components of the electric field gradient tensor, which are ordered such that $|V_{ZZ}| \geq |V_{YY}| \geq |V_{XX}|$. Q is the nuclear quadrupole moment, and values of -40.1 and 104 mb were used for ^7Li and ^{23}Na , respectively.^[35] In addition to the magnitude, the calculations also generate the sign of C_Q . However, the sign of C_Q cannot be determined from the experimental data presented in this work; therefore, when comparing calculated and experimental quadrupolar couplings, we refer only to the magnitude of the calculated C_Q .

3 | RESULTS AND DISCUSSION

3.1 | Crystal structures

Crystal structures for the six dicarboxylate salts are shown in Figure 1. The structures considered are lithium benzenedicarboxylate ($\text{Li}_2\text{C}_8\text{H}_4\text{O}_4$, Li_2BDC), lithium naphthalenedicarboxylate ($\text{Li}_2\text{C}_{12}\text{H}_6\text{O}_4$, Li_2NDC), lithium biphenyldicarboxylate ($\text{Li}_2\text{C}_{14}\text{H}_8\text{O}_4$, Li_2BPDC), sodium benzenedicarboxylate ($\text{Na}_2\text{C}_8\text{H}_4\text{O}_4$, Na_2BDC), sodium naphthalenedicarboxylate ($\text{Na}_2\text{C}_{12}\text{H}_6\text{O}_4$, Na_2NDC) and sodium biphenyldicarboxylate monohydrate ($\text{Na}_2\text{C}_{14}\text{H}_{10}\text{O}_5$, $\text{Na}_2\text{BPDC}\cdot\text{H}_2\text{O}$). All structures shown are from the literature with the exception of $\text{Na}_2\text{BPDC}\cdot\text{H}_2\text{O}$, which was solved by single-crystal XRD analysis in this work. Each structure features metal carboxylate layers

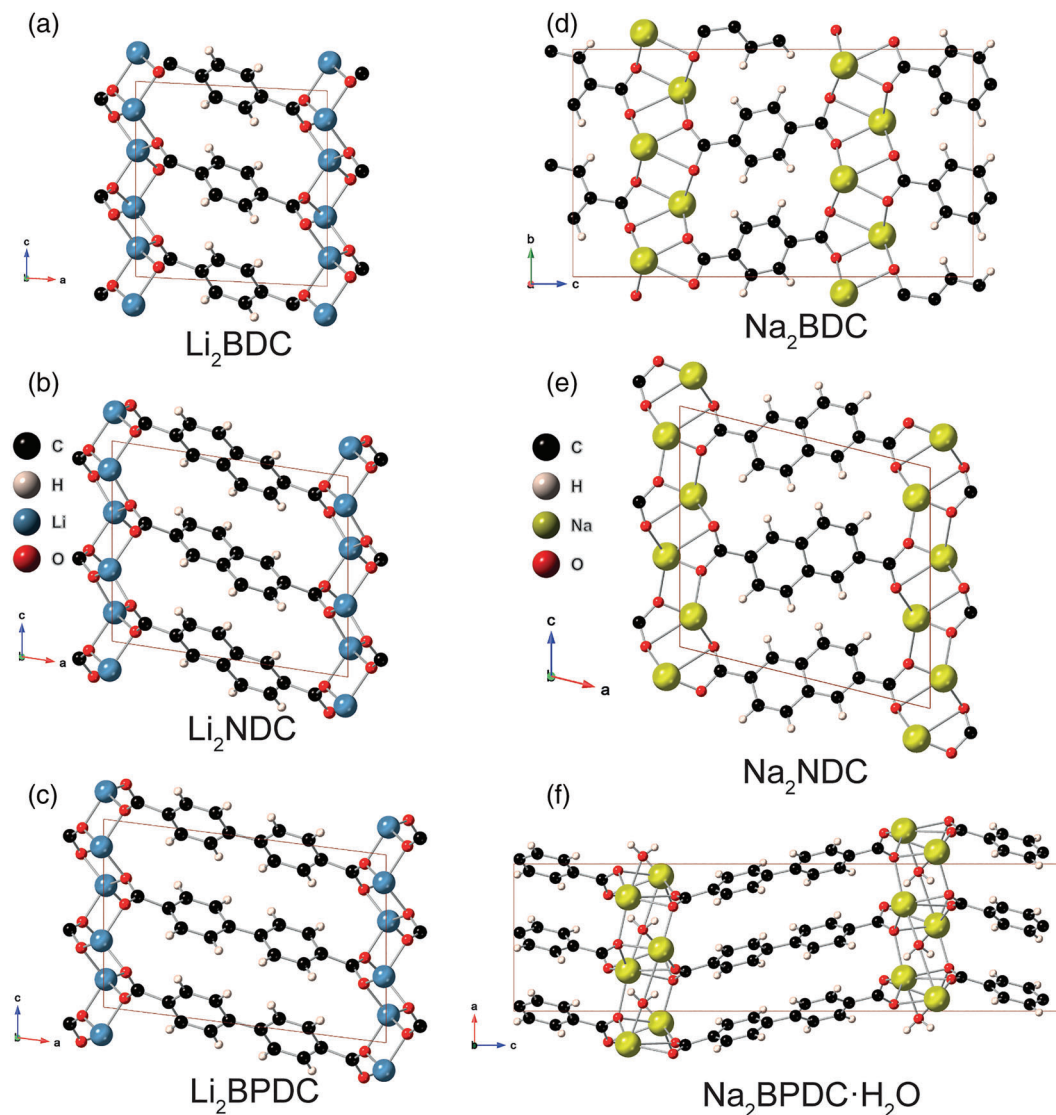


FIGURE 1 Crystal structures of (a) Li_2BDC [23], (b) Li_2NDC [24], (c) Li_2BPDC [25], (d) Na_2BDC [19], (e) Na_2NDC [14] and (f) $\text{Na}_2\text{BPDC}\cdot\text{H}_2\text{O}$ (this work)

separated by diagonally offset organic linkers. The diagonal offset results in a herringbone-like stacking of the organic linkers. In the sodium salts, there is considerable further offset in both non-stacking dimensions, creating a double herringbone arrangement. In $\text{Na}_2\text{BPDC}\cdot\text{H}_2\text{O}$, a water molecule resides within the sodium carboxylate layer, increasing the inter-ionic distance between neighbouring sodium ions relative to the other sodium salts. Consequently, the inter-ring distance between the organic backbone units is also increased by $\sim 2 \text{ \AA}$.

With respect to the metal ions, all lithium compounds have a single, crystallographically distinct lithium site, and the sodium compounds (Na_2BDC , Na_2NDC and $\text{Na}_2\text{BPDC}\cdot\text{H}_2\text{O}$) have two, one and two sodium sites, respectively. Li_2BDC possesses four carbon sites due to an inversion-type symmetry on the organic linker. This

inversion-type symmetry is also found in Li_2NDC and Li_2BPDC , resulting in six and seven carbon sites, respectively. Although the sodium dicarboxylates feature a similar herringbone stacking arrangement observed in the lithium analogues, neither Na_2BDC nor $\text{Na}_2\text{BPDC}\cdot\text{H}_2\text{O}$ retain the inversion-type symmetry, and as a result, all carbon sites are crystallographically distinct. In contrast, Na_2NDC possesses six carbon sites, similar to its lithium analogue.

In general, the structures of the metal carboxylate layers are similar across all compounds, with one key difference between lithium and sodium compounds observed in the metal oxide layer. In the lithium compounds, lithium ions form almost planar layers, with each lithium ion coordinated to four oxygen atoms in a distorted tetrahedral geometry. In contrast, in the sodium

compounds, the alkali ions are forced out of planarity by the increased ionic radius while also coordinating to between four and six oxygen atoms in more distorted geometries.

The six dicarboxylate salts were synthesised as powders according to the procedures described in Section 2.1. Experimental PXRD patterns are shown in Figure S1 together with simulated patterns based on the crystal structures shown in Figure 1. For the BDC and NDC salts, very good agreement is observed between the experimental and simulated patterns. For Li_2BPDC , small deviations in some of the peak positions and intensities are observed above $20^\circ 2\theta$. We note that in the original structure solution, the sample was found to contain multiple components, suggesting that this material can crystallise in multiple polymorphs.^[25] The simulated PXRD data are based upon the structure determined for the major component, but it is possible that other components with subtly different structures could also be present in the powder sample. For $\text{Na}_2\text{BPDC}\cdot\text{H}_2\text{O}$, the experimental PXRD pattern for the powder sample shows some minor differences with a simulated pattern for the single-crystal structure determined in the current work. We note that a slightly different crystal structure was previously reported by Choi et al.,^[11] which is characterised by a planar ring arrangement in contrast to the twisted ring arrangement in the structure from the current work (Figure S2). A multi-phase Le Bail fit shows that $\text{Na}_2\text{BPDC}\cdot\text{H}_2\text{O}$ crystallised as a mixture (Figure S3). The mixture is composed of a dominant orthorhombic phase, consistent with the structure solved by SCXRD in this work, and a further monoclinic phase consistent with the structure reported by Choi et al.^[11]

3.2 | ^{13}C solid-state NMR spectroscopy

^{13}C cross polarisation (CP) MAS NMR spectra for each of the six organic salts are shown in Figure 2. Each spectrum shows characteristic resonances expected for the carboxylate and ring carbons present in the structures. For the lithium salts, the carboxylate resonances are shifted to higher chemical shift than those of the respective sodium salts; this can be attributed to the depletion of electron density at the carboxylate carbon due to the reduced electronegativity of the sodium ion and the longer Na—O bond lengths in the sodium salts. For Li_2BDC , all of the crystallographically distinct carbon sites are resolved. For Li_2NDC , Li_2BPDC , Na_2BDC and Na_2NDC , some of the crystallographically distinct ring carbons are unresolved. Despite chemical equivalence between some aromatic carbons, there remain minor variations in their local bonding environments arising from crystallographic

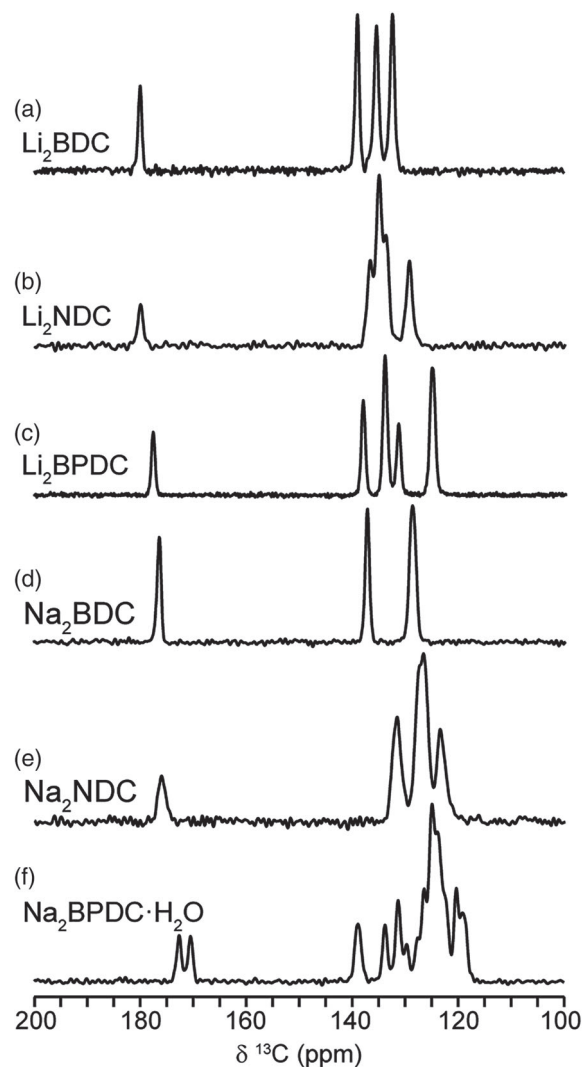


FIGURE 2 ^{13}C CPMAS NMR spectra of (a) Li_2BDC , (b) Li_2NDC , (c) Li_2BPDC , (d) Na_2BDC , (e) Na_2NDC and (f) $\text{Na}_2\text{BPDC}\cdot\text{H}_2\text{O}$. Spectra collected at 16.4 T and 15 kHz MAS, except 'c', which was collected at 16 kHz

inequivalence and, in particular, position relative to adjacent rings. This produces small but measurable differences in the respective chemical shifts.

For $\text{Na}_2\text{BPDC}\cdot\text{H}_2\text{O}$, the two crystallographically inequivalent carboxylate sites at either end of the BPDC ligand are resolved. As both carboxylate groups have similar chemical environments, this difference may arise due to a 5° difference in torsional angle relative to the adjacent rings (Figure S4).

3.3 | ^7Li and ^{23}Na solid-state NMR spectroscopy

Experimental ^7Li MAS and static NMR spectra for the three lithium salts are shown in Figure 3. Considering

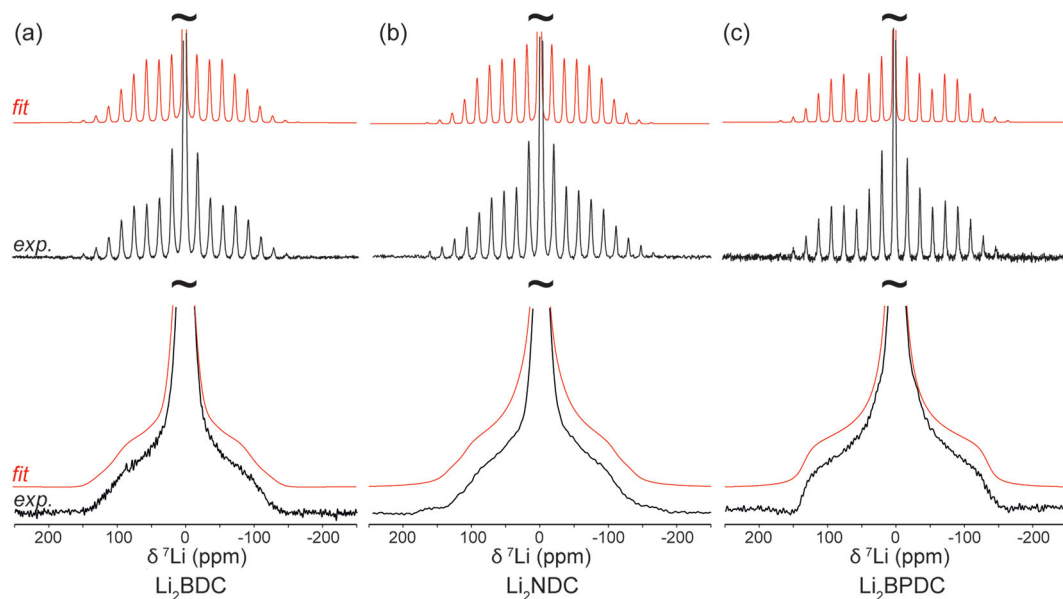


FIGURE 3 Experimental MAS (5 kHz, top) and static (bottom) ^7Li NMR of (a) Li_2BDC , (b) Li_2NDC and (c) Li_2BPDC . Spectra were collected at 16.4 T. Fits to the experimental lineshapes are shown in red. Quadrupolar parameters are given in Table 2

the MAS NMR data, each spectrum comprises a central transition resonance surrounded by satellite transition spinning sideband manifolds. For both the static and MAS data, the line shapes are broadened due to ^7Li - ^7Li homonuclear dipolar coupling interactions; this also increases the intensity of the central pair of spinning sidebands in the MAS data. Experimental chemical shift and quadrupolar parameters (summarised in Table 2) were determined by iteratively fitting the MAS and static spectra until consistent values were obtained. The measured chemical shifts of between 0.3 and 1.1 ppm are consistent with the small chemical shift range of ^7Li . The extracted C_Q values (71–75 kHz) and non-zero η_Q values between 0.5–0.9 are consistent with the distorted tetrahedral Li–O bonding geometry in the three salts.

^{23}Na MAS and MQMAS NMR spectra of the sodium salts are shown in Figure 4. ^{23}Na NMR parameters obtained from the fits are summarised in Table 3. The MAS spectrum of Na_2NDC shows a single second-order quadrupolar broadened resonance, which is consistent with the single crystallographic sodium site within the structure. The MAS NMR spectra of Na_2BDC and $\text{Na}_2\text{BPDC}\cdot\text{H}_2\text{O}$ both show second-order quadrupolar broadened line shapes with features suggesting the presence of more than one unresolved resonance. In the corresponding MQMAS spectra, two sites are observed for both materials, in agreement with the crystal structures. Similar to the lithium salts, the high η_Q values measured for each site are consistent with the distorted non-axially symmetric Na–O bonding environments in each structure.

TABLE 2 Summary of experimental ^7Li parameters for each lithium dicarboxylate salt

Compound	δ (ppm)	C_Q /kHz	η_Q
Li_2BDC	1.1 (3)	71 (2)	0.5 (1)
Li_2NDC	0.7 (3)	74 (5)	0.6 (1)
Li_2BPDC	0.3 (6)	75 (5)	0.9 (1)

3.4 | DFT calculations

In order to link experimental solid-state NMR data to the crystal structures, DFT calculations were performed. Prior to the calculation of NMR parameters, crystal structures were geometry optimised. As discussed in Section 1, DFT often fails to adequately describe long-range non-bonding interactions. This results from the absence of van der Waals interactions in commonly used exchange correlation functionals and can lead to unrealistic cell expansions during the geometry optimisation procedure. One way to address this is to constrain the unit cell parameters to the experimental values during the geometry optimisation; however, in recent years, a number of semi-empirical dispersion correction (SEDC) schemes have been developed which modify the DFT-calculated energy using an empirically derived dispersion correction.^[36] For the carboxylate salts considered in this work, much of the structure is defined by covalent bonds within the organic ligands and ionic bonds within the Li–O and Na–O layers, which should be well described by DFT. However, it is not clear to what extent weak interactions

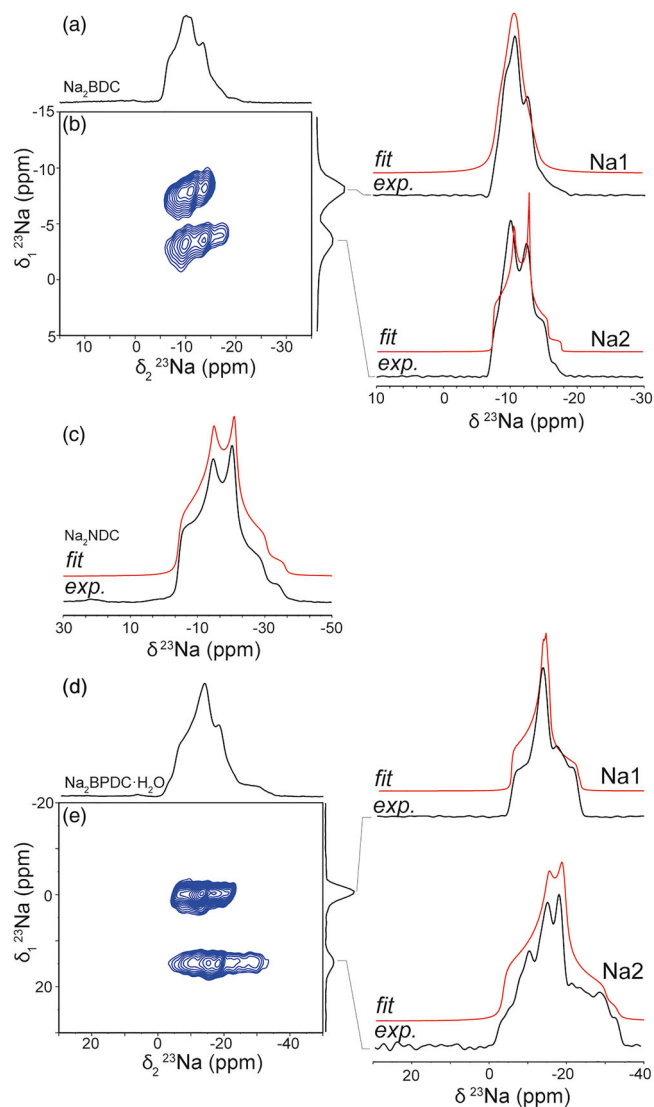


FIGURE 4 ^{23}Na MAS NMR spectra for (a) Na_2BDC , (c) Na_2NDC and (d) $\text{Na}_2\text{BPDC}\cdot\text{H}_2\text{O}$, and ^{23}Na MQMAS spectra of (b) Na_2BDC and (e) $\text{Na}_2\text{BPDC}\cdot\text{H}_2\text{O}$. Line shapes extracted from the MQMAS spectra are shown on the right together with fits (shown in red). All spectra were recorded at 9.4 T and 12.5 kHz MAS

TABLE 3 Summary of experimental ^{23}Na NMR parameters for the sodium dicarboxylate salts

Compound	Site	δ (ppm)	C_Q / MHz	η_Q
Na_2BDC	1	-7.0(8)	1.3(1)	0.7(1)
	2	-5.5(6)	1.6(1)	0.5(1)
Na_2NDC	1	-4.0(5)	2.3(1)	0.6(1)
$\text{Na}_2\text{BPDC}\cdot\text{H}_2\text{O}$	1	-4.8(4)	1.7(1)	0.9(1)
	2	-2.8(6)	2.2(1)	0.8(1)

between adjacent ligands (e.g., π - π interactions between stacked or partially stacked rings) may influence the structure. For this reason, four different geometry

TABLE 4 Labels used for different optimisation methods in this work

Method	SEDC scheme	Optimisation constraints
A	None	Unit cell parameters and heavy atom positions fixed to experimental values. Proton positions allowed to vary
B	None	Unit cell parameters fixed to experimental values. All atom positions allowed to vary
C	None	Unit cell parameters and all atom positions allowed to vary
D	G06	Unit cell parameters and all atom positions allowed to vary

optimisation procedures were explored in order to assess how well different methods account for any dispersion interactions from the perspectives of both the optimised structure and the calculated NMR parameters. In Method A, the unit cell parameters were constrained to experimental values, and only proton positions were allowed to vary, such that the relative arrangement of the ligands and metal oxide layers were constrained to the experimental data. In Method B, unit cell parameters were constrained to experimental values, while all atomic positions were allowed to vary. In Method C, all atom positions and unit cell parameters were allowed to vary, while in Method D, all atom positions and the unit cell parameters were allowed to vary under the G06 SEDC scheme.^[34] A summary of optimisation methods can be found in Table 4.

Figure 5 shows percentage changes in unit cell parameters and volumes for both of the optimisation methods where the unit cell was allowed to vary (Methods C and D). Method C resulted in significant increases of unit cell volume of between 6% and 20% for all structures (Figure 5a). For most structures, the expansion is anisotropic with a dominant contribution to the volume expansion along one particular dimension. In all cases, the dominant expansion dimension is parallel to the axis defining the herringbone stacking arrangement of the organic linkers. As an example, following optimisation via Method C, the distance between the centre of two stacked aromatic rings in Na_2NDC increased by 21.6% from 3.617 to 4.399 Å (Figure S5a,b).

Figure 5b shows changes in unit cell parameters and volume for structures optimised via Method D. These results show a clear contrast to Method C, with slight contractions in unit cell volume observed for all compounds. It is notable that the magnitudes of the contractions in unit cell volume (2–6%) are significantly smaller than the expansions observed for Method C (6–20%),

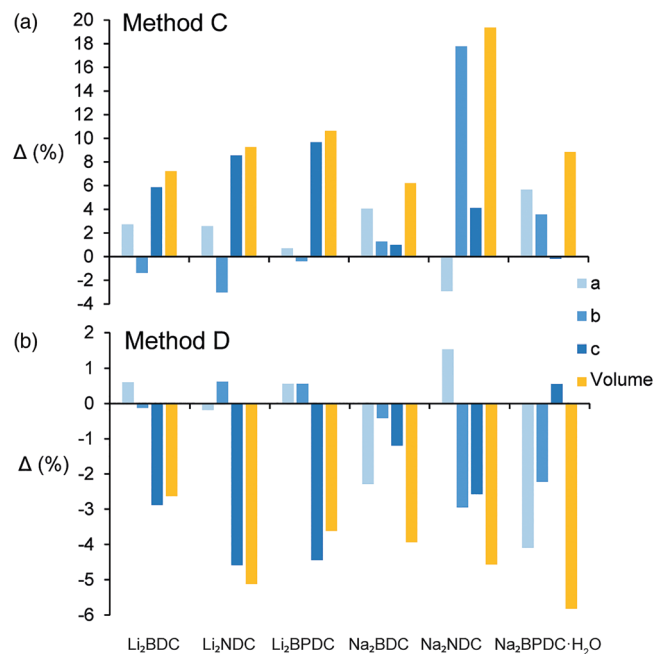


FIGURE 5 The percentage change in unit cell dimensions (a, b, c) and cell volume between the unoptimised and optimised structures for optimisation Method C (a) and Method D (b) for each of the dicarboxylate salts (structures available in Figure 1). Full details of optimisation method can be found in Table 4

indicating smaller overall changes to the structure during the optimisation process. It is also notable that the same dimensions are responsible for the contraction of the unit cell volume that were responsible for the unit cell expansions in Method C. Using the same example, the distance between the same aromatic rings in the Na₂NDC structure decreased by 2.8% from 3.617 to 3.513 Å (Figures S5a and S4c).

The expansions observed for Method C are consistent in magnitude to a study using a layered metal organic framework (MOF) which saw an ~12% increase in unit cell volume using the equivalent geometry optimisation procedure.^[37] This is notably larger than the expansion observed in a recent study (~3%) that used the same geometry optimisation procedure on aluminophosphate (AlPO) compounds; however, AlPOs feature large 3D covalent bonding networks which are comparatively more rigid than the layered intramolecular bonding nature of metal carboxylate salts.^[38] The contractions observed for Method D are consistent with the layered MOF and AlPO studies, where smaller magnitude contractions were seen (~1%) with the inclusion of an SEDC scheme as part of the geometry optimisation.^[38] A recent study of organoaluminium complexes observed large contractions of ~8% using the same optimisation method; however, the structures considered were molecular complexes with an even greater structural dependence on weak intermolecular interactions.^[39]

The clear differences in total unit cell volume change between the two methods highlight the importance of weak π - π non-bonding interactions in defining the inter-ring stacking distance within the lithium and sodium carboxylate structure considered here. Furthermore, they show that the inclusion of an SEDC scheme in the optimisation procedure can effectively address the large expansions observed in the standard DFT approach. When an SEDC scheme is used, the unit cell changes are much smaller, but there is an overall tendency for structural contraction. One potential explanation for this could be thermal effects in the diffraction-derived structures which are typically obtained at temperatures between 90 and 150 K. In contrast, the DFT calculations do not account for temperature effects and therefore will not reproduce any thermal expansion that may be present in real structures under experimental conditions at finite temperatures.^[38] However, since the main dimension of contraction is also the one that defines the organic linker stacking, the observed contractions could also suggest that the SEDC scheme slightly overestimates the strength of the π - π interactions between the linkers.

In addition to changing the unit cell size, it is important to consider how the atomic positions within the unit cell change during geometry optimisation. This can be explored through comparison of simulated PXRD patterns for the optimised structures (Figures S6 and S7). The position of reflections can be solely determined from the unit cell dimensions; therefore, in Methods A and B where the unit cell is fixed, no changes in positions are observed; however, the reflection intensities do vary. Unsurprisingly, the largest deviations from the experimental PXRD data are observed for Method C, where in addition to a tendency for peaks to shift to lower 2θ (consistent with the unit cell expansion); the relative positions and intensities of peaks also change significantly for some structures. This shows that the significant unit cell expansions observed for this method are also accompanied by changes in the relative arrangements of the ligands and metal carboxylate layers. It is also noteworthy that although the methods incorporating fixed unit cells and SEDC generally show closer agreement with the experimental data, there are still notable changes in relative peak positions with those methods where the heavy atom positions and unit cell dimensions are allowed to vary.

3.5 | Calculated ¹³C NMR parameters

Correlations of the experimental chemical shifts with the calculated chemical shieldings for each salt from each of the optimisation methods are shown in Figure 6. All

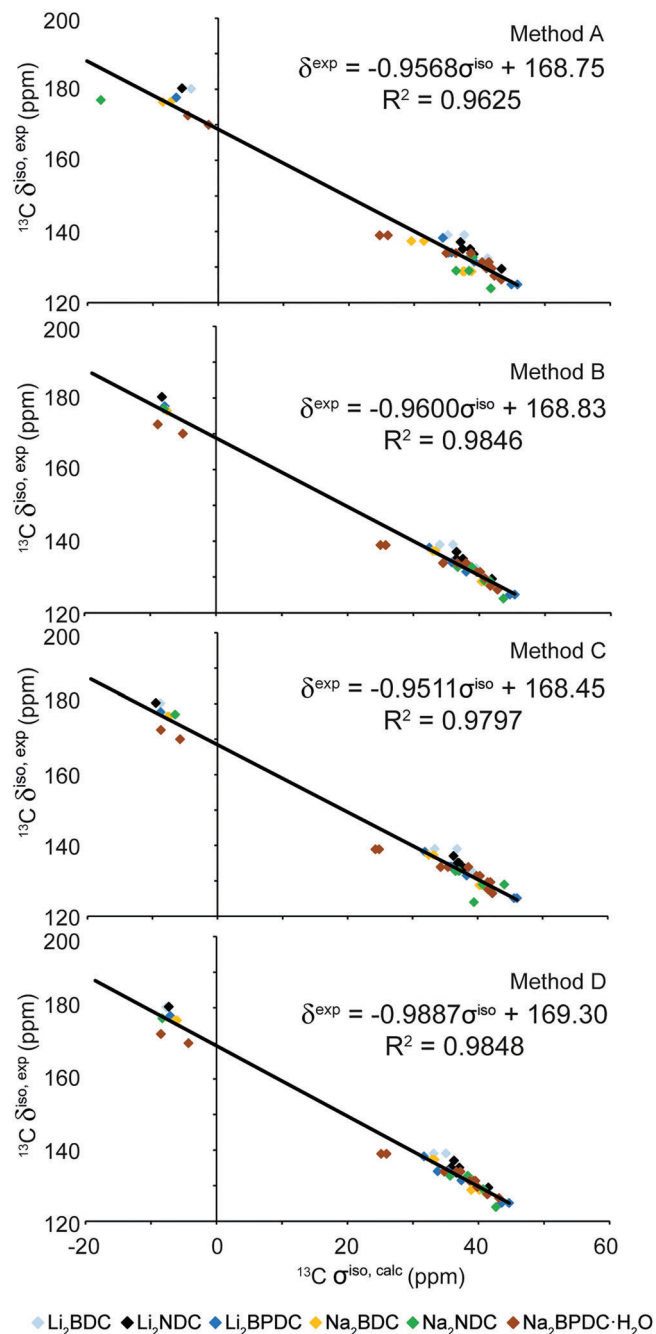


FIGURE 6 Plot of ¹³C calculated chemical shielding and experimental isotropic chemical shift. Full details of optimisation method can be found in Table 4

optimisation methods give linear correlations with gradients close to -1 . Method A gives the weakest correlation ($R^2 = 0.9625$) compared with the other methods, which highlights that proton optimisation alone is not sufficient to give good agreement for ¹³C NMR. In particular, Na₂NDC shows particularly poor agreement, with the data point corresponding to the carboxylate group ($\sigma^{\text{iso, calc}} = -18$ ppm) lying furthest from the line of best fit. Methods B–D show improved correlations with

similar scatter, suggesting that the optimisation approach does not have a significant impact on the ¹³C chemical shieldings, providing that all atoms are optimised. However, for Na₂BPDC·H₂O, the ¹³C chemical shielding appears to be underestimated by each optimisation method, particularly the carboxylate and quaternary carbons $\sigma^{\text{iso, calc}}$ approximately -10 and 25 ppm, respectively. This consistent underestimation may be related to the water molecules in this structure which are in close proximity to these carbons which may have some static disorder or may undergo dynamics within the structure which is not accounted for by the DFT calculations.

Interestingly, the large unit cell expansion observed for Method C does not appear to significantly affect the overall correlation. Similarly, the small unit cell contractions observed for Method D also do not reduce the overall agreement. For all methods, the reference shielding based on the correlations are within ± 1 ppm of each other. Overall, these results show that while different optimisation strategies alter the geometry of the structures, they do not appear to significantly affect the ¹³C chemical shifts, provided that all atoms are optimised.

3.6 | Calculated quadrupolar NMR parameters

To aid comparison of the calculated parameters and experimental quadrupolar parameters, experimental C_Q and η_Q values were converted to the three individual components of the EFG tensor, V_{XX} , V_{YY} and V_{ZZ} . Magnitudes of the experimental and calculated tensor components are correlated in Figure 7. Full summaries of the calculated quadrupolar parameters together with simulated ⁷Li and ²³Na NMR spectra are shown in Tables S1 and S2 and Figures S8–S10.

Figure 7 shows that the calculated ⁷Li quadrupolar NMR parameters give reasonable agreement with experiment for all methods with a tendency for calculated tensor components to be overestimated by between 21% and 35%. Considering the calculated ²³Na NMR parameters, Method A gives very poor agreement which is primarily due to the calculated Na₂NDC data significantly overestimating the magnitude of the tensor components. Inspection of the sodium carboxylate layer in the optimised structure from Method A reveals significant asymmetry in the bond lengths around the sodium site (Figure S11), with considerable variation in Na–O bond lengths from 1.811 to 3.095 Å. As Method A only optimises proton positions, this suggests that the position of the sodium ion in the experimental diffraction structure

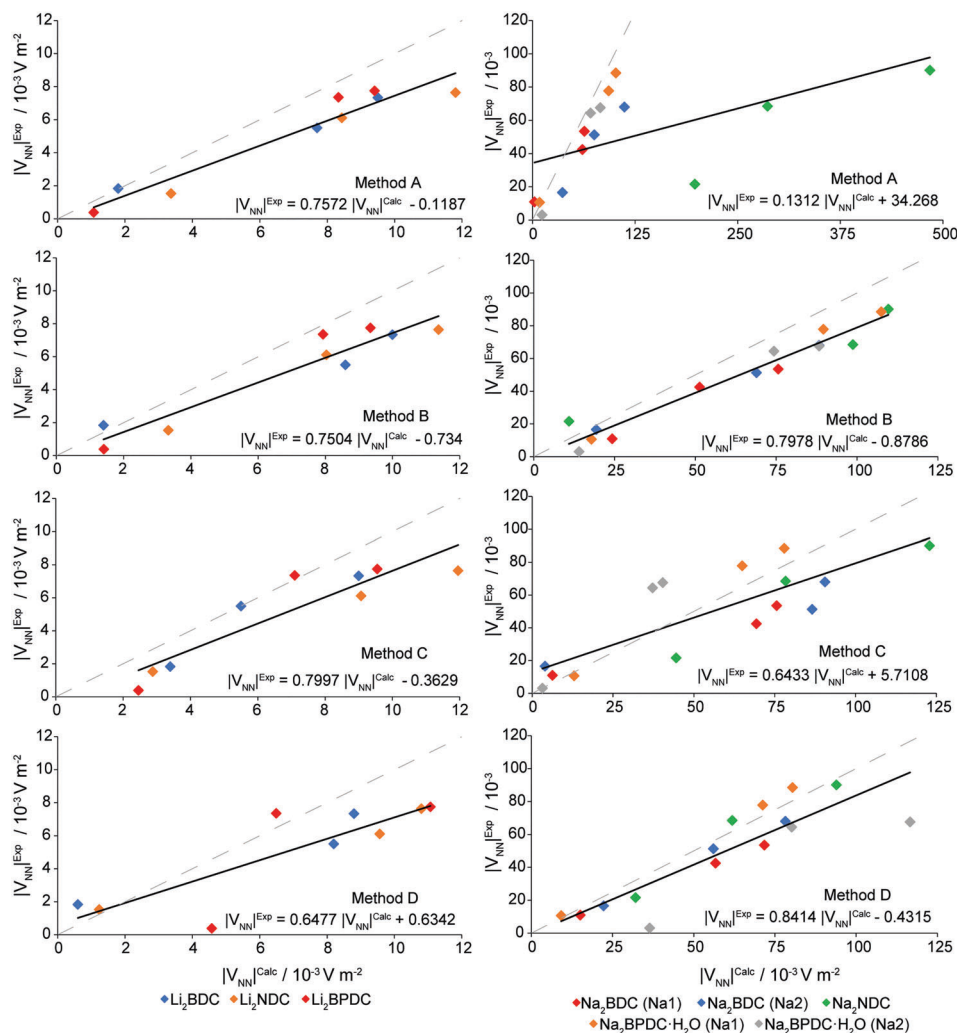


FIGURE 7 Plot of calculated and experimental ${}^7\text{Li}$ (left) and ${}^{23}\text{Na}$ (right) quadrupolar tensor components for lithium and sodium dicarboxylates. $|V_{\text{NNI}}| = V_{\text{XX}}, V_{\text{YY}}$ and V_{ZZ} . Grey dashed line represents perfect agreement. Full details of optimisation method can be found in Table 4

is not accurately defined. The observation is consistent with the ${}^{13}\text{C}$ NMR data (Figure 6) where the shielding of the carboxylate carbon, which is situated closest to the sodium carboxylate layer, is also poorly reproduced by the DFT calculations using Method A. For the other optimisation methods where the position of heavy atom positions are allowed to vary, a significant change in the Na–O bond lengths is observed with bond lengths converging to a range of 2.401 to 2.624 Å for Method D (Figure S11). The calculated quadrupolar tensor components for these structures are in much better agreement with experiment, further suggesting that the Na position in the diffraction structure is not accurately defined. However, considering the simulated PXRD data (Figure S7), Method A gives reasonable agreement with experiment and is significantly better than Method C. This highlights the high sensitivity of NMR to

the local structure and shows the benefits of NMR crystallography in considering both the local and long-range structure.

Considering the rest of the ${}^{23}\text{Na}$ NMR calculations, there is again a tendency for overestimation of predicted tensor components by a similar amount to the ${}^7\text{Li}$ NMR calculations. In a ${}^{25}\text{Mg}$ NMR study of magnesium acetate clusters, C_Q values were also overestimated by approximately 30% on average using a DFT approach equivalent to Method B. Despite this, η_Q parameters were predicted reasonably well.^[40] In contrast, ${}^{27}\text{Al}$ C_Q values for organoaluminium complexes were generally underestimated in comparison to experiment,^[39] whereas for aluminophosphate frameworks, a closer correlation was obtained.^[38] In a recent study of organic hydrogen-bonded systems, calculated ${}^{35}\text{Cl}$ C_Q values were overestimated in a comparison with experiment, and better

agreement was obtained by empirically optimising the damping parameter in the SEDC used. However, in the same study, ^{14}N and ^{17}O C_Q values were reproduced approximately equally well using both modified and unmodified SEDC schemes. The apparent overestimation of calculated EFG tensor components in the current study is therefore likely to originate from a number of factors. First, the limited number and range of values means that it is difficult to draw strong conclusions. A wider study of a larger number of structures and wider range of C_Q values would enable a better statistical picture to be obtained. Second, as shown by Holmes and Schurko,^[41] the agreement between calculated and experimental quadrupolar parameters can be highly nucleus dependent, even within the same materials. Empirical optimisation of the SEDC damping parameter can increase the overall accuracy of calculated C_Q values, but the optimal parameter is likely to be dependent on both the nucleus and structure type under consideration. Overall, for the organic carboxylate salts studied here, the results show that the choice of optimisation method does not significantly change the accuracy of calculated chemical shielding or quadrupolar parameters. It is noteworthy

that the accuracy of calculated ^{13}C chemical shifts is slightly reduced for optimisations where only proton positions are varied, despite the fact that simulated PXRD patterns show best agreement with experimental PXRD. In contrast, optimisations where all atom positions are allowed to vary typically lead to measurable changes in the simulated PXRD patterns but closer overall agreement between calculated and experiment ^{13}C chemical shifts. This highlights the differences between PXRD and solid-state NMR in terms of sensitivity to local versus long-range structural effects.

3.7 | Polymorphism and hydration behaviour of Na_2NDC and Na_2BPDC

While the anhydrous phase of Na_2NDC has been discussed in previous sections, a tetrahydrate form, $\text{Na}_2\text{NDC}\cdot 4\text{H}_2\text{O}$, has also previously been reported.^[26] In the current work, this phase was identified as a single crystal from a slow crystallisation, but it was not possible to produce enough material for solid-state NMR analysis. However, during the course of experiments, a new phase

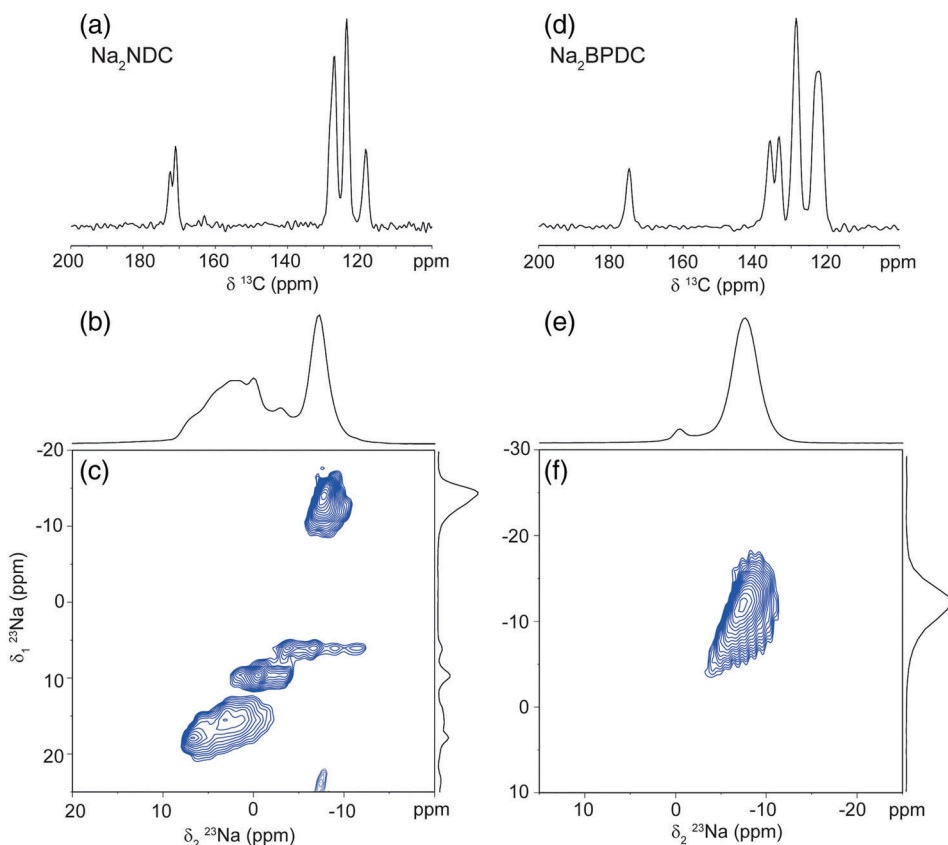


FIGURE 8 ^{13}C CPMAS (a, d), ^{23}Na MAS (b, e) and ^{23}Na MQMAS (c, f) NMR spectra of the uncharacterised Na_2NDC and anhydrous Na_2BPDC respectively. All spectra recorded at 16.4 T and 12.5 kHz MAS except the ^{13}C CPMAS NMR spectra (a, d) which were recorded at 15 kHz MAS

was identified as a powder. The sample was prepared by a similar method to anhydrous Na_2NDC except that after initial filtration, the filtrate was concentrated before being washed with methanol forming a milky suspension. The resulting suspension was then filtered again, and the recovered powder was dried in vacuo. The PXRD pattern of this phase (Figure S12) does not match either of the known anhydrous Na_2NDC or $\text{Na}_2\text{NDC}\cdot 4\text{H}_2\text{O}$ phases. The ^{13}C CPMAS NMR spectrum (Figure 8a) shows two carboxylate resonances at 171.1 and 172.5 ppm, which suggests the structure has a different symmetry from the known anhydrous phase. The resonances corresponding to the ring carbons show a similar overall form to those observed for the anhydrous phase (Figure 2e) but are shifted to lower chemical shift by approximately 5 ppm. The ^{23}Na MAS spectrum (Figure 8b) shows a complex unresolved lineshape. The ^{23}Na MQMAS spectrum (Figure 8c) reveals this is made up of at least five separate resonances, with two relatively sharp resonances at $\delta_1 = 6.0$ and 9.7 ppm, and broader resonances at -13.9 , 15.7 and 18.0 ppm (extracted lineshapes can be seen in Figure S13). In a high-field MQMAS spectrum recorded at 23.5 T (Figure S14), the resolution of the sharp resonances in δ_1 increases, but the broad resonances at 15.4 and 18.6 ppm remain unresolved. This could suggest the presence of more than one phase in the sample, with an ordered crystalline phase giving rise to the sharp resonances and a more disordered phase (possibly not observed in the PXRD pattern) giving rise to the broader resonances. Thermogravimetric Analysis (TGA) of the new Na_2NDC phase shows a mass loss of around 10.6% between 100°C and 200°C (Figure S15). This corresponds to a mass loss of 34.05 g mol^{-1} for a tetrahydrate stoichiometry ($\text{Na}_2\text{NDC}\cdot 4\text{H}_2\text{O}$, $\text{MW} = 332.21\text{ g mol}^{-1}$) or 31.40 g mol^{-1} for a dihydrate stoichiometry ($\text{Na}_2\text{NDC}\cdot 2\text{H}_2\text{O}$, $\text{MW} = 296.18\text{ g mol}^{-1}$). For the tetrahydrate stoichiometry, the mass loss is very close to that of two H_2O molecules (36.03 g mol^{-1}); however, it is unlikely that only two H_2O molecules would be lost with the other two remaining in the structure to the decomposition temperature of 600°C. For the dihydrate stoichiometry, the mass loss does not correspond to an integer multiple of H_2O molecules. A possible explanation could be that the sample corresponds to a mixture of a dihydrate Na_2NDC phase and a (possibly disordered) anhydrous Na_2NDC phase, which is not observed in the PXRD pattern. This would be consistent with the observation of the broad and sharp resonances in the MQMAS spectrum and would result in a reduced TGA mass loss where H_2O molecules are only lost from the hydrated portion of the sample.

Considering Na_2BPDC , as discussed above, the previously reported crystal structure and the one determined

in this work both correspond to monohydrate phases with small structural differences characterised by the twisting of the BPDC linker. Choi et al.^[11] prepared anhydrous Na_2BPDC through thermal treatment of $\text{Na}_2\text{BPDC}\cdot\text{H}_2\text{O}$ at 120°C in vacuo, although a crystal structure was not reported. To investigate the structure of anhydrous Na_2BPDC , a sample was prepared by a similar procedure to that reported by Choi et al.^[11] and different from that used in this work for $\text{Na}_2\text{BPDC}\cdot\text{H}_2\text{O}$, where instead of crystallisation the sample was filtered and heated in a vacuum oven at 120°C for 12 h. The PXRD pattern (Figure S16) confirms that this treatment changes the structure and shows close agreement with that reported for anhydrous Na_2BPDC by Choi et al.^[11] The ^{13}C CPMAS NMR spectrum (Figure 8d) shows one carboxylate and four ring carbon resonances which is consistent with the number of chemically distinct carbons in the structure, suggesting there is only one molecular configuration. The carboxylate resonance is shifted by ~ 10 ppm to higher chemical shift than the monohydrate phase, which is consistent with a reduction in the electron density on the carboxylate group, as may be expected if the loss of water molecules leads to stronger sodium-carboxylate bonds. In contrast, the ring carbon resonances are shifted by ~ 5 ppm to lower chemical shift. In view of the twisted configuration of the ligands in the monohydrate structure, this could suggest a difference in the relative orientations of rings in the ligands or closer packing of the rings leading to increased ring current shielding. The ^{23}Na MAS NMR spectrum (Figure 8e) shows a featureless broad lineshape centred at -7.5 ppm, together with a low intensity resonance at -0.3 ppm, which is attributed to a minor impurity. The lineshape shows a broadened 'tail' to low frequency which is characteristic of a distribution of quadrupolar interactions, indicative of disorder. The ^{23}Na MQMAS NMR spectrum (Figure 8f) confirms this, as a single resonance is observed which is broadened in both dimensions indicating that the Na ions have a disordered local environment. Overall, these results indicate that dehydration of $\text{Na}_2\text{BPDC}\cdot\text{H}_2\text{O}$ leaves a structure characterised by some degree of long-range order (as evidenced from the PXRD pattern) but that the ordering of sodium ions in the sodium carboxylate layers is disrupted leaving local disorder. The closer packing of the ligands indicated by the reduction in chemical shift of the ring carbons suggests that the overall layered structure may be retained.

4 | CONCLUSIONS

This work has presented a systematic structural study of model lithium and sodium battery organic anode

materials by NMR crystallography. For the six samples studied, the calculation of NMR parameters using diffraction structures enables distinct chemical and crystallographic environments to be assigned in ^{13}C , ^7Li and ^{23}Na solid-state NMR spectra. Comparison of the DFT-calculated ^{13}C , ^7Li and ^{23}Na NMR parameters shows that the choice of optimisation method does not significantly affect the accuracy of the calculated NMR parameters, providing that all atoms are optimised. For proton-only optimisations, slightly poorer agreement between calculated and experimental ^{13}C chemical shifts is observed. Additionally, this optimisation method highlights the sensitivity of the ^{23}Na quadrupolar interaction to the local chemical environment, which is very poorly reproduced for Na_2NDC . Allowing all atom positions to vary changes the Na–O bond lengths, resulting in much better agreement with experiment. The DFT geometry optimisations also show that despite the strong ionic bonds holding the layered structures together, weak non-bonding interactions between adjacent ligands are also important in defining the structure, and large unit cell expansions are observed if these are not accounted for. This problem can be mitigated by either fixing the unit cell parameters to experimental values during the structural optimisation or by including a SEDC scheme. Both of these methods give comparable accuracy in terms of calculated ^{13}C , ^7Li and ^{23}Na NMR parameters.

This work suggests that it should be possible to extend the NMR crystallographic approach to the study of lithiation and sodiation mechanisms in organic anode materials, where the known structures of the parent phases could serve as a starting point for investigating the currently unknown structures of the electrochemically reduced forms. However, in this case, the lithiation/sodiation process may result in changes to the unit cell parameters, even if the overall ordering of the ligands and Na-carboxylate layers is retained. Therefore, fixing the unit cell parameters to experimental values for the parent phase may impose unrealistic constraints on the system; instead, the preferable optimisation method would be to allow the unit cell parameters to vary in conjunction with a SEDC scheme to account for ligand–ligand interactions.

In addition, we have also investigated the hydration behaviour of Na_2NDC and Na_2BPDC . For Na_2NDC , we have observed a new hydrated phase which is likely to be a dihydrate, in contrast to the known tetrahydrate structure. We have also shown that the hydrated phase of Na_2BPDC exhibits disorder within the metal-dicarboxylate layer, which perhaps explains why the structure of this phase has so far not been solved by XRD. It seems that the sodium dicarboxylate salts have

a greater propensity to form hydrated phases than lithium dicarboxylate salts—this could be linked to the larger ionic radius of sodium which provides more possibility for structural incorporation of H_2O molecules into the metal-carboxylate layers. The hydrated phases may be less desirable for battery applications since the presence of even small amounts of free water in battery cells typically leads to irreversible capacity loss. However, this may not be an issue if the H_2O molecules remain within the metal-dicarboxylate layers under electrochemical cycling. Therefore, to understand how the presence of structural H_2O impacts the anode performance, further investigation is required with systematic comparisons of the anhydrous and hydrated phases. Nevertheless, we note that the specific capacity of the hydrated phases should be reduced even if no chemical effects are seen, owing to the additional mass of the H_2O molecules.

ACKNOWLEDGEMENTS

V.R.S., A.V.D., A.R.A. R.E.M. and J.M.G. are indebted to the Faraday Institution NEXGENNA project (FIRG018) for financial support. We acknowledge the support of the Leverhulme Doctoral Scholarships Programme in ‘Material Social Futures’ (grant number DS-2017-036) for the provision of a PhD studentship to T.W. We acknowledge the support from CCP-NC, funded by the Engineering and Physical Sciences Research Council (EPSRC; EP/M022501/1), and the UKCP consortium, funded by the EPSRC (EP/P025561/1). K.G. acknowledges the Leverhulme Trust (Research Project Grant Number RPG-2018-395). We are grateful to the UK Materials and Molecular Modelling Hub for computational resources, which is partially funded by the EPSRC (EP/P020194). The UK High-Field Solid-State NMR Facility used in this research was funded by EPSRC and BBSRC (EP/T015063/1) as well as, for the 1 GHz instrument, EP/R029946/1. Collaborative assistance from the Facility Management Team (Dr Trent Franks, University of Warwick) is acknowledged.


PEER REVIEW

The peer review history for this article is available at <https://publons.com/publon/10.1002/mrc.5249>.

DATA AVAILABILITY STATEMENT

The research data supporting this article can be accessed online (at <https://doi.org/10.17635/lancaster/researchdata/498>). The single-crystal XRD structure for $\text{Na}_2\text{BPDC}\cdot\text{H}_2\text{O}$ determined in this work can be obtained free of charge from www.ccdc.cam.ac.uk with structure code 2120033.

ORCID

Valerie R. Seymour  <https://orcid.org/0000-0003-3333-5512>

Kieran Griffiths  <https://orcid.org/0000-0002-4509-0674>

Nathan R. Halcovitch  <https://orcid.org/0000-0001-6831-9681>

Aamod V. Desai  <https://orcid.org/0000-0001-7219-3428>

Russell E. Morris  <https://orcid.org/0000-0001-7809-0315>

A. Robert Armstrong  <https://orcid.org/0000-0003-1937-0936>

John M. Griffin  <https://orcid.org/0000-0002-8943-3835>

REFERENCES

- [1] W. Walker, S. Grugeon, H. Vezin, S. Laruelle, M. Armand, J. M. Tarascon, F. Wudl, *Electrochem. Commun.* **2010**, *12*, 1348.
- [2] D. Senthil Raja, C. C. Pan, C. W. Chen, Y. H. Kang, J. J. Chen, C. H. Lin, *Microporous Mesoporous Mater.* **2016**, *231*, 186.
- [3] M. Armand, S. Grugeon, H. Vezin, S. Laruelle, P. Ribière, P. Poizot, J. M. Tarascon, *Nat. Mater.* **2009**, *8*, 120.
- [4] L. Zhao, J. Zhao, Y. S. Hu, H. Li, Z. Zhou, M. Armand, L. Chen, *Adv. Energy Mater.* **2012**, *2*, 962.
- [5] Y. Park, D. Shin, S. H. Woo, N. S. Choi, K. H. Shin, S. M. Oh, K. T. Lee, S. Y. Hong, *Adv. Mater.* **2012**, *24*, 3562.
- [6] Y. Wang, Y. Deng, Q. Qu, X. Zheng, J. Zhang, G. Liu, V. S. Battaglia, H. Zheng, *ACS Energy Lett.* **2017**, *2*, 2140.
- [7] X. Han, C. Chang, L. Yuan, T. Sun, J. Sun, *Adv. Mater.* **2007**, *19*, 1616.
- [8] X. Han, G. Qing, J. Sun, T. Sun, *Angew. Chemie - Int. Ed.* **2012**, *51*, 5147.
- [9] L. Fédèle, F. Sauvage, S. Gottis, C. Davoisne, E. Salager, J. N. Chotard, M. Becuwe, *Chem. Mater.* **2017**, *29*, 546.
- [10] L. Fédèle, F. Sauvage, J. Bois, J. M. Tarascon, M. Becuwe, *J. Electrochem. Soc.* **2014**, *161*, 46.
- [11] A. Choi, Y. K. Kim, T. K. Kim, M. S. Kwon, K. T. Lee, H. R. Moon, *J. Mater. Chem. A* **2014**, *2*, 14986.
- [12] N. Ogihara, T. Yasuda, Y. Kishida, T. Ohsuna, K. Miyamoto, N. Ohba, *Angew. Chemie - Int. Ed.* **2014**, *53*, 11467.
- [13] T. Yasuda, N. Ogihara, *Chem. Commun.* **2014**, *50*, 11565.
- [14] J. M. Cabañero, V. Pimenta, K. C. Cannon, R. E. Morris, A. R. Armstrong, *ChemSusChem* **2019**, *12*, 4522.
- [15] C. Bonhomme, C. Gervais, F. Babonneau, C. Coelho, F. Pourpoint, T. Azaïs, S. E. Ashbrook, J. M. Griffin, J. R. Yates, F. Mauri, C. J. Pickard, *Chem. Rev.* **2012**, *112*, 5733.
- [16] S. E. Ashbrook, D. McKay, *Chem. Commun.* **2016**, *52*, 7186.
- [17] P. Hodgkinson, *Prog. Nucl. Magn. Reson. Spectrosc.* **2020**, *118–119*, 10.
- [18] N. Ogihara, N. Ohba, Y. Kishida, *Sci. Adv.* **2017**, *3*, 1.
- [19] J. A. Kaduk, *Acta Crystallogr. Sect. B Struct. Sci.* **2000**, *56*, 474.
- [20] O. V. Dolomanov, L. J. Bourhis, R. J. Gildea, J. A. K. Howard, H. Puschmann, *J. Appl. Crystallogr.* **2009**, *42*, 339.
- [21] G. M. Sheldrick, *Acta Crystallogr. Sect. A Found. Adv.* **2015**, *71*, 3.
- [22] G. M. Sheldrick, *Acta Crystallogr. Sect. C Struct. Chem.* **2015**, *71*, 3.
- [23] Y. Y. Liu, J. Zhang, L. X. Sun, F. Xu, W. S. You, Y. Zhao, *Inorg. Chem. Commun.* **2008**, *11*, 396.
- [24] D. Banerjee, S. J. Kim, J. B. Parise, *Cryst. Growth des.* **2009**, *9*, 2500.
- [25] D. Banerjee, L. A. Borkowski, S. J. Kim, J. B. Parise, *Cryst. Growth des.* **2009**, *9*, 4922.
- [26] V. Medabalmi, K. Ramanujam and V. Ramkumar, CCDC 1558952: CSD Communications, **2018**, <https://doi.org/10.5517/ccdc.csd.cc1pb6s0>
- [27] A. E. Bennett, C. M. Rienstra, M. Auger, K. V. Lakshmi, R. G. Griffin, *J. Chem. Phys.* **1995**, *103*, 6951.
- [28] P. K. Madhu, A. Goldbourn, L. Frydman, S. Vega, *Chem. Phys. Lett.* **1999**, *307*, 41.
- [29] M. D. Segall, P. J. D. Lindan, M. J. Probert, C. J. Pickard, P. J. Hasnip, S. J. Clark, M. C. Payne, *J. Phys. Condens. Matter* **2002**, *14*, 2717.
- [30] C. J. Pickard, F. Mauri, *Phys. Rev. B - Condens. Matter Mater. Phys.* **2001**, *63*, 2451011.
- [31] J. P. Perdew, K. Burke, M. Ernzerhof, *Phys. Rev. Lett.* **1996**, *77*, 3865.
- [32] J. R. Yates, C. J. Pickard, F. Mauri, *Phys. Rev. B - Condens. Matter Mater. Phys.* **2007**, *76*, 1.
- [33] B. Hammer, L. B. Hansen, J. K. Nørskov, *Phys. Rev. B - Condens. Matter Mater. Phys.* **1999**, *59*, 7413.
- [34] S. Grimme, *J. Comput. Chem.* **2006**, *27*, 1787.
- [35] P. Pyykko, *Mol. Phys.* **2008**, *106*, 1965.
- [36] J. Klimeš, A. Michaelides, *J. Chem. Phys.* **2012**, *137*, 120901.
- [37] B. K. Chang, N. C. Bristowe, P. D. Bristowe, A. K. Cheetham, *Phys. Chem. Chem. Phys.* **2012**, *14*, 7059.
- [38] S. Sneddon, D. M. Dawson, C. J. Pickard, S. E. Ashbrook, *Phys. Chem. Chem. Phys.* **2014**, *16*, 2660.
- [39] C. Cross, L. Cervini, N. R. Halcovitch, J. M. Griffin, *Magn. Reson. Chem.* **2021**, *59*, 1024.
- [40] V. R. Seymour, S. P. Day, G. Scholz, K. Scheurell, D. Iuga, J. M. Griffin, E. Kemnitz, J. V. Hanna, M. E. Smith, *ChemPhysChem* **2018**, *19*, 1722.
- [41] S. T. Holmes, R. W. Schurko, *J. Phys. Chem. C* **2018**, *122*, 1809.

SUPPORTING INFORMATION

Additional supporting information may be found in the online version of the article at the publisher's website.

How to cite this article: T. Whewell, V. R. Seymour, K. Griffiths, N. R. Halcovitch, A. V. Desai, R. E. Morris, A. R. Armstrong, J. M. Griffin, *Magn Reson Chem* **2022**, *1*. <https://doi.org/10.1002/mrc.5249>